

# Mesoscopic Structure of *meso*-Tetrakis(4-sulfonatophenyl)porphine J-Aggregates

Norberto Micali,<sup>†</sup> Francesco Mallamace,<sup>\*,§</sup> Andrea Romeo,<sup>¶</sup> Roberto Purrello,<sup>△</sup> and Luigi Monsù Scolaro<sup>\*,§,¶</sup>

*Istituto di Tecniche Spettroscopiche, ITS–CNR, Messina, Italy, Dipartimento di Fisica, Università di Messina, Messina, Italy, INFN, Sezione di Messina, Italy, Dipartimento di Chimica Inorganica, Chimica Analitica e Chimica Fisica, Università di Messina, and Istituto di Chimica dei Prodotti Naturali (ICTPN–CNR), Sezione di Messina, Messina, Italy, and Dipartimento di Scienze Chimiche, Catania, Italy*

Received: June 10, 1999; In Final Form: March 7, 2000

Samples containing J-aggregates formed by the porphyrin *meso*-tetrakis(4-sulfonatophenyl)porphine ( $H_2TPPS_4^{4-}$ ) were studied by a combination of elastic (ELS) and dynamic (DLS) light scattering techniques. Aggregation was fostered by lowering the pH and increasing the ionic strength ( $I$ ; selected experimental conditions: (i) pH = 0.7; (ii) pH = 2.8,  $I$  = 0.5 M; (iii) pH = 0.7,  $I$  = 2 M). The ELS data suggest the presence of self-similar structures, whose fractal dimension are  $d_f$  = 1.7, 2.13, and 2.09 (for case i, ii, and iii, respectively). The DLS experiments indicate the presence of large (1–1.5  $\mu$ m)-, medium (100–200 nm)-, and small (3–6 nm)-sized aggregates. An aggregation number ( $N$ ) ranging between 6 and 32 was calculated for the smaller components, whereas a range of  $10^5$  to  $10^6$  was found in the case of the large clusters. The aggregation kinetics were followed by the resonance light scattering technique. The average aggregation time and the growth models, as derived from the ELS experiments, are in agreement with the Derjaguin–Landau–Verwey–Overbeek (DLVO) theory for aggregation of colloidal particles. The experimental findings point out the different ability of  $H^+$  and  $Na^+$  in driving the final mesoscopic structure.

## I. Introduction

Self-assembling processes of molecular components into large supramolecular structures are primarily investigated because of their involvement in many fundamental physicochemical as well as biological processes. The possibility of changing the mesoscopic structure of the resulting species through a proper choice of the molecular components opens the way to the design and synthesis of materials capable of exhibiting specific properties and functions.<sup>1–3</sup> From this point of view, porphyrins are well suited building blocks because, depending on their electronic and steric properties, they can spontaneously self-assemble into dimers or higher aggregates through noncovalent interactions.<sup>4</sup> In particular, water-soluble porphyrins are very interesting because aggregation can be conveniently controlled by screening the charge repulsion by changes in the ionic strength ( $I$ ) and pH. London's dispersive forces acting between adjacent porphyrin cores are mainly responsible for the observed interactions.<sup>5,6</sup> Many relevant physicochemical properties of this class of compounds, including spectroscopic and photophysical features, are strictly dependent on their aggregation state; for example, the special pair is a chlorophyll dimer, which is the electron donor in the bacterial reaction center,<sup>7–10</sup> and circular organized arrays of bacteriochlorophylls are key constituents in the light-harvesting bacterial complex LH2.<sup>11</sup>

On the basis of these properties the aggregation of a large number of chromophores in organized arrays is a challenging

problem, and the formation of porphyrin wheels has recently been achieved by solvent evaporation.<sup>12,13</sup> A different approach is based on the electrostatic interactions between charged porphyrins and oppositely charged polymeric matrices, which act as template supports (e.g. DNA,<sup>14–16</sup> RNA,<sup>17,18</sup> and polypeptides<sup>19–23</sup>). In the absence of a template, the formation of highly ordered J- and/or H-aggregates has been reported.<sup>24–32</sup> The H- and J-aggregates correspond to the limiting cases of parallel monomeric units stacked *face-to-face* or *edge-to-edge*, respectively. Indeed, the formation of J-aggregates is common for a large variety of aromatic compounds (i.e., cyanine dyes,<sup>33,34</sup> xanthenes,<sup>35</sup> and polycyclic aromatic hydrocarbons<sup>36,37</sup>). According to the excitonic splitting theory,<sup>38,39</sup> H-aggregates exhibits a blue-shifted Soret band, whereas J-aggregates are characterized by a red-shifted and intense absorption band. This spectroscopic feature is sharp in comparison to that of the monomer, and this phenomenon has been explained in terms of motional narrowing, which averages the local inhomogeneities.<sup>40</sup>

In particular, the porphyrin *meso*-tetrakis(4-sulfonatophenyl)porphine ( $H_2TPPS_4^{4-}$ ) (Figure 1) has recently received particular attention because its diacid form ( $H_4TPPS_4^{2-}$ ), under particular experimental conditions, is able to form J-aggregates in which the zwitterionic porphyrins are arranged in a side-by-side stacking structure, exhibiting a strong and narrow red-shifted absorption band at 490 nm.<sup>25–28</sup> Different experimental evidence has indicated an average aggregation number of 11 (by UV/vis spectroscopy)<sup>24</sup> or 22 monomers (by fluorescence anisotropy)<sup>28</sup> for the J-aggregate, even if the observation of an excitation-dependent emission in the fluorescence spectra of aggregated  $H_4TPPS_4^{2-}$  has been considered as indicative of polydispersity in the aggregates.<sup>28</sup> The involvement of quite a large number of porphyrins ( $N \approx 10^4$ – $10^5$ ) in the aggregates has also been

\* Corresponding author. Fax: +39-090-393756. E-mail: Monsu@chem.unime.it.

<sup>†</sup> Istituto di Tecniche Spettroscopiche.

<sup>‡</sup> Dipartimento di Fisica.

<sup>§</sup> INFN.

<sup>¶</sup> Dipartimento di Chimica Inorganica.

<sup>△</sup> Dipartimento di Scienze Chimiche.

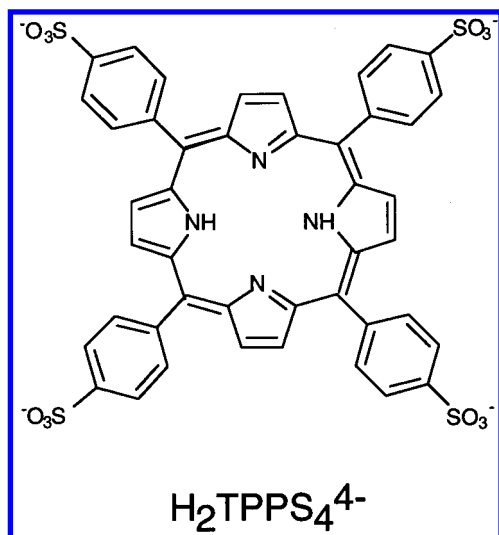


**Figure 1.** Structure of *meso*-tetrakis(4-sulfonatophenyl) porphine ( $\text{H}_2\text{TPPS}_4^{4-}$ ).

addressed by resonance light scattering (RLS)<sup>26,41,42</sup> experiments, which have pointed out the presence of an extremely weak network in solution whose structure has not been yet characterized.<sup>32</sup>

Recently, using a combination of elastic (ELS) and dynamic (DLS) light scattering techniques, we have reported that on increasing  $I$ , a dicationic porphyrin (*trans*-bis(4-*N*-methylpyridinium)diphenylporphine, *trans*- $\text{H}_2\text{Pagg}$ ) aggregates, forming large (in the mesoscopic range), rigid, and almost monodispersed clusters, with a fractal structure,<sup>43</sup> whose aggregation mechanism is controlled by the salt concentration.<sup>44</sup> The kinetics of the aggregation process have been studied by UV/vis spectroscopy, taking advantage of the quite large difference between the spectral features of the monomeric and aggregated species.<sup>45,46</sup>

Fractal geometry and scaling concepts are currently used to describe the structure and the dynamics of colloidal systems.<sup>47</sup> The mass ( $M$ ) of a fractal object is related to its radius ( $R$ ) through the scaling law  $M \sim R^{d_f}$ , where  $d_f$  is the fractal or Hausdorff dimension.<sup>48</sup> According to its definition, this coefficient is not an integer number and its value ranges between 1.7 and 2.5. Computer simulations have related this parameter to the different growth processes: (i) percolation and diffusion-limited aggregation (DLA),  $d_f = 2.5$ ; (ii) diffusion-limited cluster-cluster aggregation (DLCCA),  $d_f = 1.75$ ; and (iii) reaction-limited aggregation (RLA),  $d_f = 2.1$ .<sup>47,49</sup> Therefore the fractal dimension is a signature either of the aggregation kinetic and of the cluster structure. A variety of both experimental and computational techniques have been used to determine this parameter.<sup>47,49</sup> In the early studies, scattering techniques (light, X-rays, neutrons) were exploited to gather information on geometrical aspects of aggregated species, but nowadays they represent a powerful experimental tool to also investigate the dynamics of these systems. The combination of different scattering techniques gives a detailed relationship between the hydrodynamic and static properties of an aggregate. Furthermore, these techniques have the advantage of being noninvasive and requiring a fairly low concentration of scattering objects in solution. In the present case, this aspect is important because it has been reported that an increase of the porphyrin concentration causes an increase in the complexity of the aggregated species in solution.<sup>25,32</sup>

The lack of structural information on the clusterization process involving aggregated  $\text{H}_4\text{TPPS}_4^{2-}$ , which leads to the formation of the weak network just mentioned, prompted us to study this

system under different experimental conditions. In the present paper, we report the results obtained by a combination of ELS and DLS techniques on these J-aggregates. The experimental findings suggest that  $\text{H}_4\text{TPPS}_4^{2-}$  oligomerizes, giving clusters in which some of the porphyrins (6–32) maintain the arrangement typical of J-aggregates, which in turn is responsible for the observed UV/vis spectroscopic features. These smaller aggregates can be regarded as the building blocks for growing much larger objects, and the entire system behaves as a colloidal solution. It is well established that different regimes of aggregation kinetics (reversible and irreversible) can occur in colloids depending on the interaction potential between particles, which can be controlled by varying  $I$  and pH. Therefore, the kinetics of aggregation have been also followed by RLS, and the resulting data were compared with those reported for the *trans*- $\text{H}_2\text{Pagg}$  porphyrin, with the aim of confirming the mesoscopic size and the consequent colloidal nature of these porphyrin solutions.

## II. Experimental Section

**(i) Materials.** Aqueous solutions of the porphyrin  $\text{H}_2\text{TPPS}_4^{4-}$  were prepared by dissolving the tetrasodium salt (Aldrich) in dust-free Millipore water. Stock solutions were stored in the dark and used within a week of preparation. The range of concentration ( $5\text{--}20 \times 10^{-6}$  M) used in our experiments was determined spectrophotometrically using  $\epsilon_{412} = 3.55 \times 10^5 \text{ M}^{-1}\text{cm}^{-1}$  at the Soret maximum in water.<sup>25</sup> Aggregation was started by addition of the proper amount of a concentrated HCl and/or NaCl solution, up to the required concentration, directly in the cylindrical silica cell used in the scattering measurements. To avoid or minimize dust contamination, special care was taken by filtering all the stock solutions through 0.22- $\mu\text{m}$  Millipore filters.

**(ii) Methods.** The UV/vis spectra were obtained on a Hewlett-Packard model 8452 A diode array spectrophotometer. The RLS experiments were performed on a Jasco model FP-750 spectrofluorimeter using a synchronous scan protocol with right-angle geometry.<sup>15,41</sup> The kinetic measurements (RLS) were followed at fixed wavelength by mixing the reagents in a silica cell in the thermostated compartment of the instrument. The average aggregation time,  $\tau_E$ , defined according to the following equation:

$$\tau_E = \frac{\int_0^\infty \langle I(t) \rangle dt}{\langle I(0) \rangle} \quad (1)$$

was evaluated by numerical integration of the intensity of the scattered light  $I(t)$  versus time (where  $\langle I(t) \rangle$  and  $\langle I(0) \rangle$  are the intensity mean values at time  $t$  and at  $t = 0$ , respectively). The reported  $\tau_E$  values were averaged from 3–5 different kinetic runs. We wish to emphasize that the kinetic of the aggregation depends on the history of the sample. To obtain comparable results, we used the same concentrated porphyrin stock solution, which was previously filtered through a 0.22- $\mu\text{m}$  Millipore syringe filter, for an entire set of kinetic runs. Prolonged aging leads to different induction times in the kinetic traces (see *Results*) and, a different order of mixing reagents can give different results. For better reproducibility, a known volume of a concentrated stock solution of porphyrin was added as last reagent to a solution containing the proper amount of HCl and NaCl.

**Elastic and Dynamic Light Scattering.** The ELS measurements were performed on a computerized homemade goniometer in the angular range  $20^\circ \leq \theta \leq 150^\circ$ , corresponding to scattering

wavevectors  $4.58 \leq q \leq 25.5 \mu\text{m}^{-1}$  ( $q = (4\pi n/\lambda) \sin(\theta/2)$ , with  $n$  the refractive index,  $\lambda$  the incident wavelength, and  $\theta$  the scattering angle). The integration time for each angle was 5 s.

The DLS measurements were obtained in the same angular range used for ELS measurements. The scattered light was collected through optical fibers matched with a digital Hamamatsu R942 photomultiplier cooled at  $-30^\circ\text{C}$ . The signal was sent to a Malvern 4700 submicron particle analyzer system (eight parallel correlators at different sampling times) and the intensity–intensity correlation function  $g^2(\tau)$  was measured in the time range  $10 \mu\text{s} \leq \tau \leq 1\text{s}$ , using a typical acquisition time of 200 s. The exciting light source in both types of experimental setup was a 17 mW polarized HeNe laser (632.8 nm). To avoid experimental artifacts due to fluorescence, an interference filter was set on the observation path during the measurements. Porphyrin samples (2 mL) were placed in a Burchard cylindrical quartz cell (Hellma) and held inside a homemade thermostatic system. The temperature controller provided a constant value of 298 K with an accuracy of 0.01 K. The light scattering data were collected on at least seven different samples to check for reproducibility, and the results were consistent within the experimental error.

**ELS Data Analysis.** The experimental determination of the fractal dimension  $d_f$  is based on the measurements of the scattered intensity  $I(q)$  as function of the exchanged wavevector  $q$ .<sup>47</sup> The measured intensity  $I(q)$  is related to the form factor  $P(q)$  and to the structure factor  $S(q)$  by the equation:<sup>50</sup>

$$I(q) \propto P(q)S(q) \quad (2)$$

In our experiments the form factor  $P(q)$  is close to unity because the porphyrin is the monomer and because of the  $q$  range used.<sup>43,50</sup> Furthermore, it can be demonstrated that for a fractal aggregate,  $S_M(q) \propto S(qR)$ ,<sup>51</sup> where  $S_M(q)$  is the structure factor of a cluster of mass  $M$  and radius  $R$ . The mass  $M$  of the cluster is related to the mass of the monomeric unit through the equation  $M = M_0 k$ , where  $k$  is the number of monomers of mass  $M_0$  and size  $R_0$ . Under the condition  $qR_0 \ll 1$  and  $qR \gg 1$  (Porod condition), eq 2 simplifies to:

$$I(q) \propto S(q) \propto q^{-d_f} \quad (3)$$

The value of the fractal dimension  $d_f$  can be determined from the slope of the straight line obtained by plotting the intensity  $I(q)$  as a function of  $q$  on a double logarithmic plot.

**DLS Data Analysis.** The DLS technique is commonly used to determine the diameter of submicrometric dispersed particles by measuring their diffusion coefficients.<sup>50</sup> The correlation function of the scattered light intensity,  $g^2(\tau)$ , is given by:

$$g^2(\tau) \propto \exp(-Dq^2\tau) \quad (4)$$

Such a correlation function of the scattered field is proportional to the density–density correlation function.<sup>50</sup> In the case of a monodispersed noninteracting system, the hydrodynamic radii  $R_H$  of the particles can be obtained through the Einstein–Stokes relationship:

$$D = (k_B T) / (6\pi\eta R_H) \quad (5)$$

where  $\eta$  is the solvent viscosity at the temperature  $T$  and  $k_B$  is the Boltzmann constant. In the case of a polydispersed sample, the measured correlation function is a superimposition of exponential functions with different decay rates.<sup>52</sup> The distribution of these decay rates can be obtained through a Laplace inversion of the field correlation function  $g^1(\tau)$ . To perform this

analysis, we used a discrete multiexponential nonnegative least-squares fit to invert the experimental data (NNLS).<sup>53,54</sup>

### III. Results

The favorable spectroscopic features of  $\text{H}_2\text{TPPS}_4^{4-}$  have been used to investigate the solution behavior of this compound. At neutral pH, the porphyrin  $\text{H}_2\text{TPPS}_4^{4-}$  dimerizes on addition of cations and cation–crown ether complexes.<sup>55</sup> The dimerization produces red shifts of the Q-bands and of the fluorescence peaks. The  $pK_a$  for the protonation of the macrocyclic nitrogen centers of the porphyrin  $\text{H}_2\text{TPPS}_4^{4-}$  has been estimated to be 4.9.<sup>56</sup> This process leads to the diacid form  $\text{H}_4\text{TPPS}_4^{2-}$ , which exhibits a markedly different Soret band with respect to the neutral porphyrin (434 versus 412 nm). Aggregation of  $\text{H}_4\text{TPPS}_4^{2-}$  to yield a J-aggregate can be induced either by lowering pH ( $\text{pH} < 1$ ) or increasing  $I$ .<sup>28</sup> In both cases, the UV/vis spectra display a quite narrow and intense band that increases with time at 490 nm, paralleling the matching decrease of the 434 nm Soret band. The zwitterionic form of the diacid  $\text{H}_4\text{TPPS}_4^{2-}$  has been suggested as being responsible for the formation of a network of hydrogen bonds and electrostatic interactions, which stabilize this type of aggregate.<sup>25,28</sup> The occurrence of different geometrical arrangements of porphyrins (linear and angular) has been recently hypothesized.<sup>31</sup>

At high salt concentration, a slight broadening of this band is accompanied by a small bathochromic shift, which has been ascribed to the presence of aggregates of different sizes.<sup>28</sup> On increasing the porphyrin concentration, H-aggregates begin to form as evidenced by a band at 422 nm.<sup>25</sup>

In our investigations, absorption and RLS experiments were performed on samples under acidic conditions at a porphyrin concentration of  $5 \mu\text{M}$ , which ensures the presence of J-aggregates only and reproducible results.<sup>28,32</sup> Experiments conducted on more concentrated samples ( $> 10\text{--}20 \mu\text{M}$ ), even if evidencing similar spectral features and mesoscopic structures, were not reproducible, and partial precipitation of the aggregated porphyrin was detected by a slow decrease in the intensity of the Soret band at 490 nm and of the light scattering. The pH and  $I$  were adjusted with HCl and/or NaCl, and we chose the following conditions to perform our experiments: (i)  $\text{pH} = 0.7$  ( $[\text{HCl}] = 0.2 \text{ M}$ ); (ii)  $\text{pH} = 2.8$ ,  $I = 0.5 \text{ M}$ ; and (iii)  $\text{pH} = 0.7$ ,  $I = 2 \text{ M}$ . The complete aggregation of the porphyrin samples was checked by monitoring the absorbance of the 490 nm Soret band. The RLS measurements (data not shown) exhibit minima located at 490 nm and strong signals at  $\sim 500 \text{ nm}$ , which can be attributed, respectively, to intensity loss due to absorption and to the enhanced scattering of the J-aggregated porphyrin, in agreement with the results reported by Pasternack et al.<sup>26</sup>

**Elastic Light Scattering.** An aqueous solution of  $\text{H}_2\text{TPPS}_4^{4-}$  shows a low scattered intensity that is almost wave-vector independent, which is in line with the presence of monomeric porphyrins (data not shown). Addition of NaCl up to 3 M does not promote any increase of the intensity, even though the UV/vis spectral changes indicate the formation of dimers.<sup>55</sup>

In regime of complete aggregation, the different samples (i–iii) exhibit a rather large scattered intensity (benzene, used as standard scatterer, displays a wavevector independent intensity of  $\approx 10^2$  arb. un.). The double logarithmic plots of  $I(q)$  versus  $q$  (Figure 2) clearly show that the data follow a power law behavior according to eq 3. From the slopes of these straight lines, it is possible to determine the value of the fractal dimension  $d_f$ . A regression analysis of the ELS data gave the following values for the slopes  $s$ : (i)  $s = -1.70 \pm 0.05$ ; (ii)  $s = -2.13 \pm 0.04$ ; and (iii)  $s = -2.09 \pm 0.03$ . We want to



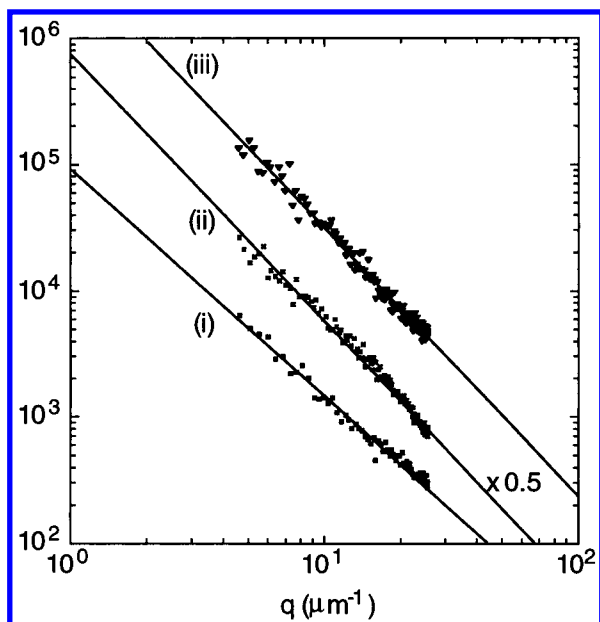


**Figure 2.** Intensity profiles  $I(q)$  versus  $q$  for aggregated  $\text{H}_2\text{TPPS}_4^{2-}$  in the regime of complete aggregation, under different experimental conditions at 298 K: (i)  $[\text{H}_2\text{TPPS}_4] = 5 \mu\text{M}$ , pH 0.7; (ii)  $[\text{H}_2\text{TPPS}_4] = 5 \mu\text{M}$ , pH 2.8,  $[\text{NaCl}] = 0.5 \text{ M}$ ; and (iii)  $[\text{H}_2\text{TPPS}_4] = 5 \mu\text{M}$ , pH 0.7,  $[\text{NaCl}] = 2 \text{ M}$ .

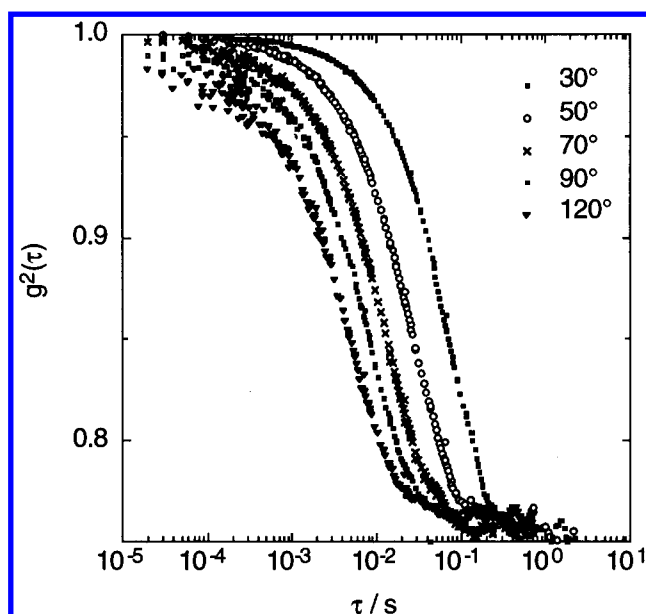


**Figure 3.** Normalized autocorrelation functions  $g^2(\tau)$  at different scattering angles for the aggregated  $\text{H}_2\text{TPPS}_4^{2-}$  under high  $I$  conditions:  $[\text{H}_2\text{TPPS}_4] = 5 \mu\text{M}$ , pH 0.7,  $[\text{NaCl}] = 2 \text{ M}$  (iii) ( $T = 298 \text{ K}$ ).

emphasize that the  $q$  range, available by using light scattering technique, is too narrow to accurately assess fractal behavior. The region of self-similarity for fractal systems is usually observed on a much larger length scale by applying a more complete form for the structure factor  $S(q)$ .<sup>57,43</sup> Nevertheless, in analogy to the porphyrin *trans*- $\text{H}_2\text{P}_{\text{agg}}$  and other model systems, such as latex suspensions and microemulsions,<sup>52</sup> it is sufficient to point out the existence of a scaling behavior by using eq 2.

**Dynamic Light Scattering.** A typical set of intensity correlation functions at various scattering angles is shown in Figure 3. The measurements were performed at different scattering angles (corresponding to different exchanged wave vectors  $q$ ) to verify the  $q$  independence of the diffusion

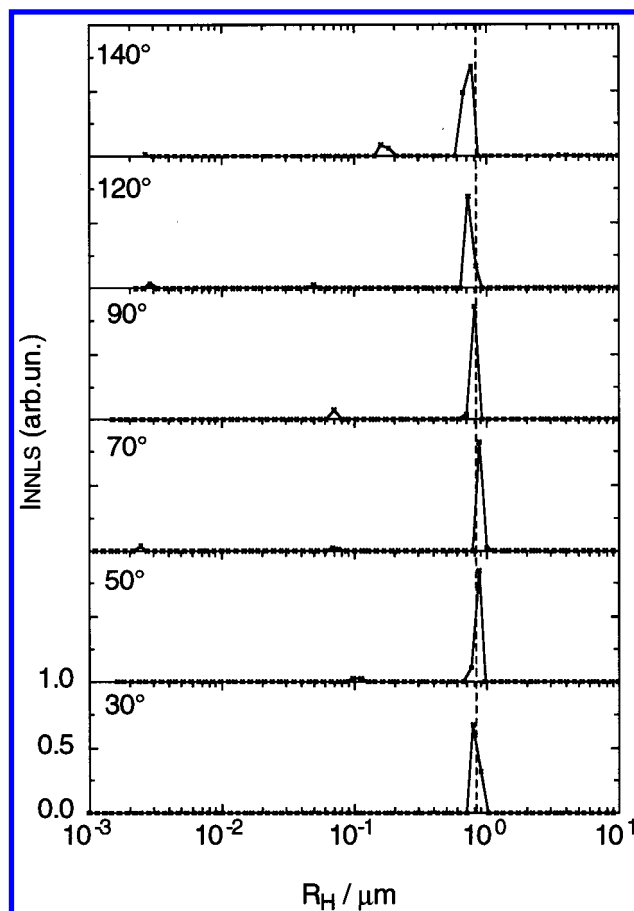


**Figure 4.** DLS analysis of the hydrodynamic radii for an aggregated sample of  $[\text{H}_2\text{TPPS}_4] = 5 \mu\text{M}$ , pH 0.7,  $[\text{NaCl}] = 2 \text{ M}$  (iii).

**TABLE 1: Diffusion Coefficients  $D$  and Hydrodynamic Radii  $R_H$  (Major Component) as Function of the Observation Angle for an Aggregated Sample of  $[\text{H}_2\text{TPPS}_4] = 5 \mu\text{M}$ , pH 0.7 (i) at  $T = 298 \text{ K}$ <sup>a</sup>**

angle (°)	$q (\mu\text{m}^{-1})$	$10^9 D (\text{cm}^2 \text{s}^{-1})$	$R_H (\mu\text{m})$
30	6.84	$1.42 \pm 0.07$	$1.51 \pm 0.09$
50	11.2	$1.49 \pm 0.07$	$1.44 \pm 0.09$
70	15.2	$1.43 \pm 0.08$	$1.50 \pm 0.1$
90	18.7	$1.23 \pm 0.06$	$1.74 \pm 0.1$
120	22.9	$1.21 \pm 0.06$	$1.77 \pm 0.1$

<sup>a</sup> Principal component from the NNLS data analysis.

coefficient  $D$ . If such a condition is fulfilled, the measured relaxation time can be connected to the translational motion of the aggregate, and the Einstein–Stokes equation (eq 5) allows calculation of the hydrodynamic radius of the particles. The correlation functions were analyzed by a discrete multiexponential least-squares fit (NNLS) and in almost all the examined cases, the correlogram could be fitted by three exponential contributions. Figure 4 reports an example of such analysis in terms of hydrodynamic radii and relative weights under the experimental conditions (iii). Tables 1–3 summarize the numerical results in the case of the major contributions to the decay rates. Figure 5 reports the hydrodynamic radii as function of the observation angle.

In all the cases, it is possible to detect the presence of a major contribution that is centered, respectively, at (i)  $R_H = 1.59 \pm 0.3 \mu\text{m}$ , (ii)  $R_H = 1.41 \pm 0.4 \mu\text{m}$ , and (iii)  $R_H = 0.801 \pm 0.2 \mu\text{m}$ . The analysis shows that there are two minor contributions at higher frequencies: one ranges between 100 and 200 nm and the other very small one is on the average centered at 5 nm.<sup>58</sup>

**TABLE 2: Diffusion Coefficients  $D$  and Hydrodynamic Radii  $R_H$  (Major Component) as Function of the Observation Angle for an Aggregated Sample of  $[H_2TPPS_4] = 5 \mu M$ ,  $[NaCl] = 0.5 M$ , pH 2.8 (ii) at  $T = 298 K^a$**

angle ( $^\circ$ )	$q$ ( $\mu m^{-1}$ )	$10^9 D$ ( $cm^2 s^{-1}$ )	$R_H$ ( $\mu m$ )
30	6.84	$1.42 \pm 0.07$	$1.51 \pm 0.08$
50	11.2	$1.69 \pm 0.07$	$1.27 \pm 0.07$
70	15.2	$1.28 \pm 0.06$	$1.68 \pm 0.08$
90	18.7	$1.60 \pm 0.06$	$1.34 \pm 0.07$
120	22.9	$1.52 \pm 0.07$	$1.41 \pm 0.07$
140	25.5	$1.72 \pm 0.07$	$1.25 \pm 0.06$

<sup>a</sup> Principal component from the NNLS data analysis.

**TABLE 3: Diffusion Coefficients  $D$  and Hydrodynamic Radii  $R_H$  (Major Component) as Function of the Observation Angle for an Aggregated Sample of  $[H_2TPPS_4] = 5 \mu M$ , pH 0.7,  $[NaCl] = 2 M$  (iii) at  $T = 298 K^a$**

angle ( $^\circ$ )	$q$ ( $\mu m^{-1}$ )	$10^9 D$ ( $cm^2 s^{-1}$ )	$R_H$ ( $\mu m$ )
30	6.84	$2.70 \pm 0.1$	$0.793 \pm 0.05$
50	11.2	$2.49 \pm 0.1$	$0.862 \pm 0.05$
70	15.2	$2.42 \pm 0.1$	$0.884 \pm 0.05$
90	18.7	$2.66 \pm 0.1$	$0.804 \pm 0.05$
120	22.9	$2.97 \pm 0.1$	$0.722 \pm 0.05$
140	25.5	$2.89 \pm 0.1$	$0.742 \pm 0.05$

<sup>a</sup> Principal component from the NNLS data analysis.

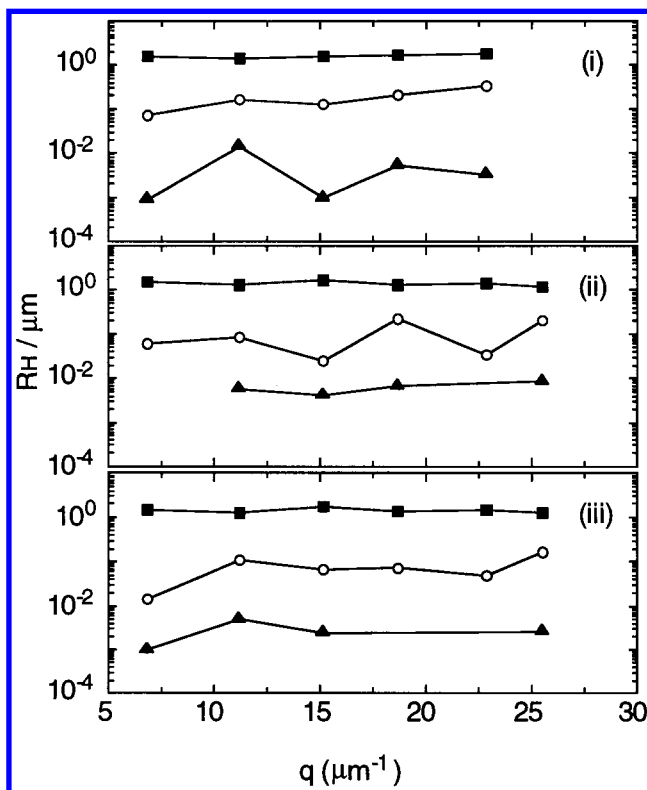


**Figure 5.** Hydrodynamic radii from the DLS analysis for aggregated  $H_2TPPS_4^{2-}$  in the regime of complete aggregation, under different experimental conditions at 298 K: (i)  $[H_2TPPS_4] = 5 \mu M$ , pH 0.7; (ii)  $[H_2TPPS_4] = 5 \mu M$ , pH 2.8,  $[NaCl] = 0.5 M$ ; and (iii)  $[H_2TPPS_4] = 5 \mu M$ , pH 0.7,  $[NaCl] = 2 M$ .

**Aggregation Kinetics.** As described previously, the formation of the J-aggregate in solution is characterized by the growth of an intense absorption band in the UV/vis at 490 nm, by the concomitant increase of the intensity  $I(q)$  obtained in ELS experiments (Figure 6), and by the build-up of a strong RLS band at  $\sim 500$  nm. These results are in line with the principle that these techniques allow for a kinetic investigation of the aggregation process. Because the size of the resulting aggregates is of the order of  $1 \mu m$  and the RLS intensity has been shown

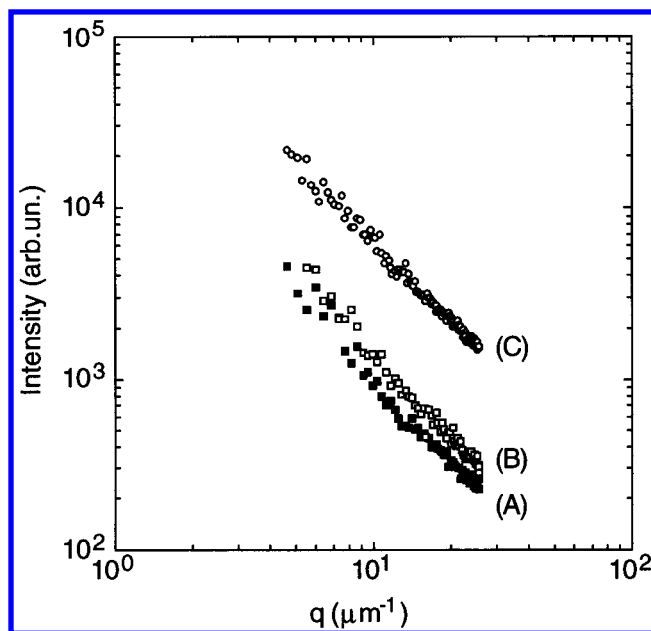


**Figure 6.** Intensity profiles  $I(q)$  versus  $q$  during the aggregation process: (A)  $t = 5$  min; (B)  $t = 20$  min; (C) after complete aggregation. Experimental conditions:  $[H_2TPPS_4] = 5 \mu M$ , pH 0.7 (i) ( $T = 298 K$ ).

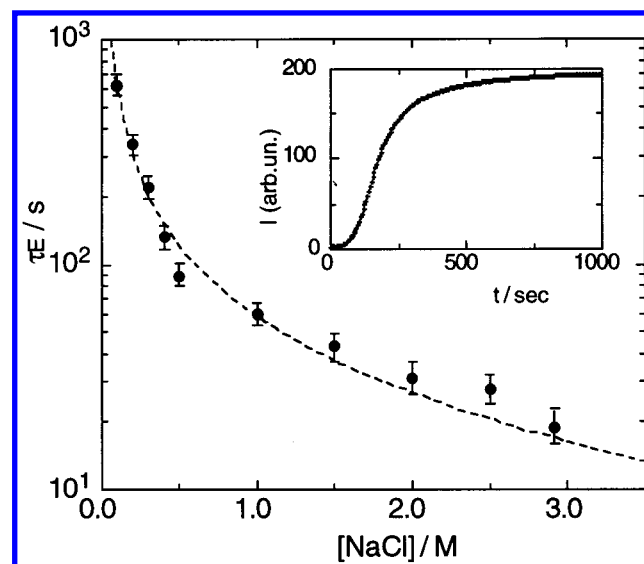


**Figure 7.** Time  $\tau_E$  for complete aggregation as a function of salt concentration determined by RLS kinetic measurements ( $[H_2TPPS_4] = 5 \mu M$ , pH 2.8,  $T = 298 K$ ). In the inset, a typical kinetic RLS profile ( $\lambda = 500$  nm) is reported ( $[H_2TPPS_4] = 5 \mu M$ , pH 2.8,  $[NaCl] = 0.5 M$ ,  $T = 298 K$ ).

to depend strongly on the size of the scattering species,<sup>42</sup> we decided to exploit this simple technique to study the kinetics of aggregation. The inset of Figure 7 shows a typical kinetic trace that exhibits a common feature for this process; that is, the presence of an induction period after which an exponential growth of the signal follows. To evaluate the kinetic data, we decided to analyze our data with the average aggregation time  $\tau_E$  defined in eq 1. Figure 7 reports a plot of this parameter obtained for the kinetics of aggregation at pH 2.8 as function of  $I$ . Interestingly, the values of  $\tau_E$  evaluated for the aggregation process started by adding HCl only ( $[HCl] > 0.1 M$ ) evidence a random behavior (data not shown).

Ageing of concentrated stock solutions of  $H_2TPPS_4^{4-}$  leads to rather different kinetic results. This observation could be explained by taking into account the formation of small

quantities of aggregates that act as nucleation sites, accelerating the clustering rates and shortening the induction times. Another interesting finding is the dependence of the aggregation process (in terms of lag-times and stability of the resulting colloidal solutions)<sup>32</sup> on the order of mixing reagents. The high local concentration of one reagent, generated in the mixing process, can be considered responsible for the observed phenomena. Again, a rather different concentration of aggregated nuclei can affect the overall growth dynamics in distinct ways. In the case of a solution at pH 1, the induction times can pass from values <30 s to values >1 h, just on reversing the mixing order.

#### IV. Discussion

**Mesoscopic Structure of the J-aggregate.** Recently, an investigation based on the combined use of ELS, small angle light scattering (SALS), and DLS has shown that the aggregated form of the porphyrin *trans*-H<sub>2</sub>P<sub>agg</sub> exhibits a fractal structure.<sup>43</sup> The ELS experiments clearly evidence that a power law of the type  $I(q) \approx q^{-d_f}$  (eq 2) is obeyed for the J-aggregates obtained under conditions (i–iii).

Interestingly, the J-aggregates formed without the addition of sodium chloride (case i) display a fractal dimension  $d_f = 1.70 \pm 0.05$ , which is indicative of a DLCCA process. Under the experimental conditions ii–iii (i.e., in the presence of Na<sup>+</sup>), the resulting aggregates have fractal dimensions  $d_f = 2.13 \pm 0.04$  and  $d_f = 2.09 \pm 0.03$ , respectively, suggesting an RLA process. This behavior is different in comparison with the porphyrin *trans*-H<sub>2</sub>P<sub>agg</sub> in which the addition of increasing amounts of sodium chloride drives the aggregation dynamics from a DLA to a DLCCA passing through an intermediate RLA.<sup>44</sup> When aggregation is started by addition of HCl only, the mesoscopic structure grows with a faster DLCCA mechanism probably because of the better ability of H<sup>+</sup> in screening the charges of the aggregated H<sub>4</sub>TPPS<sub>4</sub><sup>2-</sup>, which can be regarded as the building blocks for the larger clusters (vide infra). The observation that J-aggregate clusters retain a RLA-driven structure, even in the presence of a high Na<sup>+</sup> concentration, could be explained either by a less effective screening or by considering a role at the molecular level of the sulfonate–cation ion-pairing equilibrium on the aggregation process, in line with the observed specificity of interaction in the series of cations NH<sub>4</sub><sup>+</sup>, Na<sup>+</sup>, K<sup>+</sup>, and Ba<sup>2+</sup>.<sup>54</sup>

The diffusion coefficients  $D$  obtained by DLS measurements are almost insensitive to the scattering angles, suggesting that these values can be safely considered as translational motion. The application of the Einstein–Stokes equation to the diffusion coefficients, obtained as different contributions to the decay rate of the correlation functions, points out the presence of a major peak and two minor components. The main contribution gives a hydrodynamic radius spanning between 0.80 and 1.59  $\mu\text{m}$ , which can be assigned to the translation of large aggregates. The minor contributions could be attributed to a certain degree of polydispersity in the sample or to internal rotational motions of the aggregates. In particular, the very short relaxation time leads to an estimation of  $\sim 2.8$ – $6.3$  nm for the relative hydrodynamic radius. Under the hypothesis that this contribution can be related to a small cluster of porphyrins, we can try to calculate the number of molecules involved by two different methods. The first one is based on merely geometrical considerations, under the assumption of a rodlike shape for the J-aggregate.<sup>24</sup> Taking into account an average distance of 0.9 nm of the sulfonic end-group from the center of the macrocycle, these sizes are in agreement with a number of 6 up to 14 aligned porphyrins. In the second method, the self-similar structure of

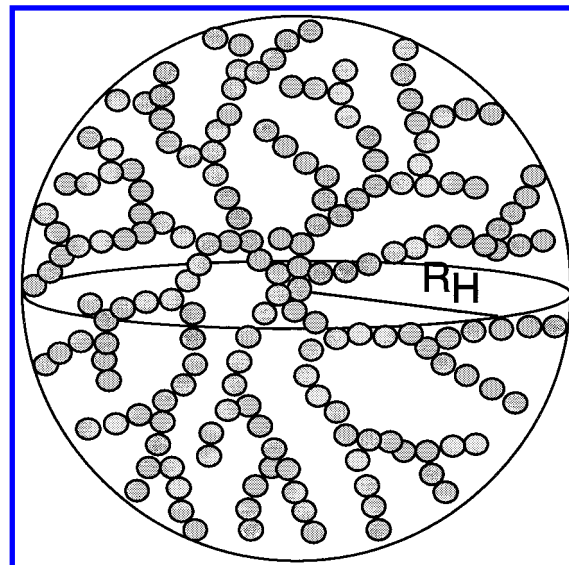


**Figure 8.** Model for the mesoscopic fractal cluster of J-aggregated H<sub>4</sub>TPPS<sub>4</sub><sup>2-</sup> in solution. The small circles represent the basic building blocks containing 6–32 porphyrin units (see text).

the aggregates and their scaling properties are exploited. The effective volume occupied by a fractal aggregate can be calculated by the equation  $V_{\text{eff}} = (4/3)\pi R^{d_f}$ . Assuming  $d_f = 2.1$ , we estimate volumes ranging from 4582 to 25160  $\text{\AA}^3$ . The hydrodynamic volume for H<sub>2</sub>TPPS<sub>4</sub><sup>4-</sup> has been evaluated as 775  $\text{\AA}^3$ ,<sup>28</sup> using Edward's theory<sup>59</sup> for the calculation of molecular volumes and Perrin's correction for the nonspherical shape of the molecule. This value leads to a number of 6 up to 32 porphyrins occupying the hydrodynamic volume of the smaller J-aggregates. Even if, in the case of these small clusters, the assumption of a fractal structure is not reliable, it is interesting to compare our results with those previously reported using spectroscopic techniques, and, as a consequence, closely related to the environment at molecular level. In the present case, the aggregation numbers  $N$  coming from DLS experiments are in fairly good agreement with previous findings obtained from UV/vis absorption spectroscopy ( $N = 11$ )<sup>24</sup> and fluorescence anisotropy lifetime measurements ( $N = 22$ ).<sup>28</sup>

The application of the second method to the major contribution of the correlation functions leads to aggregation numbers  $N$  in the range  $10^5$ – $10^6$  for the experimental conditions under investigation [(i)  $N = 6.9 \times 10^5$ , (ii)  $N = 2.8 \times 10^6$ , (iii)  $N = 7.8 \times 10^5$ ]. The aggregation number obtained for the J-aggregate formed under condition (i) is in good agreement with the value reported by Pasternack et al. for closely similar conditions.<sup>42</sup> The main difference is that, considering the J-aggregate as a cylinder, they estimated its length as  $\sim 16 \mu\text{m}$ . In a more recent investigation, exploiting the dynamic RLS technique, the same authors reported evidence for rodlike aggregates with  $\sim 10^4$  molecules along the principal axis and 20 molecules across the diameter.<sup>32</sup>

Figure 8 shows a schematic representation of the fractal model for the porphyrin mesoscopic assemblies. The smaller J-aggregates (6–32 porphyrins) can be considered as the basic building blocks for the aggregation process (the small circles). The larger structures originate by clustering of these small aggregates, which leads to self-similar objects.

**Aggregation Mechanisms.** The stability of lyophobic colloids against aggregation is described in terms of the so-called DLVO (Derjaguin–Landau–Verwey–Overbeek) theory.<sup>61,63</sup> In a colloidal suspension, the presence of a diffuse double layer surrounding the colloidal particles leads to a pair potential. This

DLVO potential,  $V(r)$ , arises from a long-range repulsive shielded ionic interaction  $V_R(r)$ , and an additional attractive short-ranged van der Waals–London interaction  $V_A(r)$ :

$$V(r) = V_R(r) + V_A(r) \quad (6)$$

Under the condition that the radius  $R_0$  of the basic particles is larger than the inverse of the Debye screening length  $k_D$  ( $R_0 k_D \gg 1$ ), the repulsive contribution is given by:

$$V_R(r) = 2\pi\epsilon\psi_0^2 \ln(1 + \exp[-2k_D R_0(r_0 - 1)]) \quad (7)$$

On the other hand, for  $R_0 k_D \ll 1$ , this contribution becomes:

$$V_R(r) = \frac{4\pi\epsilon\psi_0^2 R_0^2}{r} \exp[-k_D r_0] \quad (8)$$

where  $r_0 = r/2R_0$ ,  $r$  is the distance between the centers of the particles,  $\epsilon$  is the dielectric constant of the solvent,  $\psi_0$  is the particle surface potential, and  $k_D$  is the inverse of the Debye screening length, which is given by:

$$k_D = \left( \frac{2e^2 N 10^3}{\epsilon k_B T} I \right)^{1/2} \quad (9)$$

with  $e$  is the electronic charge,  $N$  is Avogadro's number,  $k_B$  is the Boltzmann constant,  $T$  is the absolute temperature, and  $I$  is the ionic strength.

The attractive potential is given by:

$$V_A(r) = -\frac{A}{12} \left( \frac{1}{r_0^2 - 1} + \frac{1}{r_0^2} + 2\ln(1 - r_0^{-2}) \right) \quad (10)$$

where  $A$  is the Hamaker constant.<sup>62</sup>

The total DLVO potential  $V(r)$  exhibits two minima with a barrier, and its form depends on the particle size and on the term  $R_0 k_D$ , which is dependent on  $I$  and temperature. The secondary minimum, that determines the possibility of reversible flocculation (colloidal stable state or metastable),<sup>63</sup> becomes more pronounced for larger particles and moves to shorter distances on increasing  $I$ . Irreversible aggregation is gained when a particle is able to overcome the barrier and reaches the primary minimum.

The evaluation of the probability that a particle could escape the potential barrier by Brownian motion is informative regarding the relaxation time of the colloid in its different aggregation phases. The probability per unit volume and time that particles, initially placed in the secondary minimum, could overcome the potential barrier is:<sup>64</sup>

$$\frac{dN(t)}{dt} = -\frac{1}{\tau_E} N(t) \quad (11)$$

with  $N(t)$  the number of particles in the minimum at a given time. The transition probability  $P = 1/\tau_E$  can be expressed as:

$$P = \frac{(V''_{\min} V''_{\max})^{1/2}}{12\pi^2 f} \exp[-\Delta V/k_B T] \quad (12)$$

where  $\Delta V$  is the height of the potential barrier,  $f$  is the friction coefficient, and the  $V''$  values are the second derivatives of the potential  $V(r)$  calculated at the secondary minimum and at the barrier position, respectively. Therefore, the relaxation time  $\tau_E$  is an exponential function of the height of the barrier  $\Delta V$ . A decrease of  $\Delta V$ , caused by an increase of  $I$ , causes a shortening

of the metastable state lifetime, leading to a quick aggregation passing from reversible to irreversible conditions. Our kinetic experiments performed by the RLS technique show that in the regime of RLA (case ii), an evaluation of the relaxation time  $\tau_E$  is potentially possible, and its behavior as a function of  $I$  is reported in Figure 7. A detailed analysis of these data in terms of eq 12 requires the knowledge of the molecular origin of the parameters of the interaction potential; namely, the Hamaker constant  $A$  and the surface potential  $\psi_0$ . In particular, the constant  $A$  depends on the contribution of the interparticle, the solvent–solvent, and the particle–solvent London dispersion forces.<sup>63</sup> Investigation of this issue is currently in progress in our laboratories.

The presence in the region of irreversible aggregation of two regimes, the reactive RLA and the diffusive DLCCA, can be accounted for by the DLVO potential. At high  $I$ , the repulsive part of the potential  $V_R(r)$  is completely shielded and the particles stick together by simple contact after diffusional motion, leading to DLCCA kinetics. At intermediate salt concentration, a finite barrier in the potential is present, and aggregation takes place after a thermally activated process (RLA).<sup>65–68</sup>

In the case of  $H^+$ -induced aggregation of  $H_4TPPS_4^{2-}$  (case i), the experimental observation of a DLCCA mechanism suggests that protons are able to effectively screen the repulsive component of the DLVO potential. On the contrary, when J-aggregates are formed in the presence of  $Na^+$  cations, the observed structure is driven by an RLA mechanism. Even at an high  $Na^+$  concentration, there is no evidence for a change to DLCCA. These findings are rather different than those of the salt-induced aggregation of the porphyrin *trans*- $H_2P_{agg}$ , which, as already cited, on increasing the  $I$ , aggregates, exhibiting different aggregation regimes.<sup>44</sup>

## V. Conclusions

The investigations here reported strongly indicate that J-aggregates, formed by the diacid porphyrin  $H_4TPPS_4^{2-}$ , clusterize, exhibiting self-similar structures, whose density depends on the experimental conditions. These results confirm previous suggestions on the mesoscopic nature of these species.<sup>25,32,42</sup> The DLS experiments show that the originated clusters are rather polydisperse, and the average size of these aggregates is in the range 1–1.5  $\mu m$ . Faster components in the autocorrelation functions suggest the presence of intermediate (100–200 nm) and small (3–6 nm) clusters. For these latter components, an aggregation number of a few tens of porphyrins has been calculated, in agreement with previous literature reports.<sup>24,28</sup> As a consequence, these systems can be regarded as colloidal suspensions as far as the aggregation properties are concerned. These results are of interest in comparison with the behavior of the dicationic *trans*- $H_2P_{agg}$  porphyrin. In fact, it has been shown as the latter compound aggregates on increasing the  $I$  of the solution, yielding structurally different particles.<sup>44</sup> On the other hand, the structural features of the J-aggregates formed by the zwitterionic porphyrin  $H_4TPPS_4^{2-}$  can be changed by a proper choice of pH and/or salt concentration. In the case of the *trans*- $H_2P_{agg}$ , the  $I$  plays the role of screening the positive charges of the *meso*-*N*-methylpyridinium substituents, decreasing the electrostatic repulsion between approaching molecules and increasing the attractive contribution of the London's dispersive forces.<sup>6</sup> The protonation of the nitrogen core of  $H_2TPPS_4^{4-}$  leads to a dianionic species in which the electrostatic repulsion is reduced with respect to the free base. A high concentration of either  $H^+$  or  $Na^+$  fosters the interaction between porphyrins to form clusters, even if the proton seems to be much more



effective in terms of rate of aggregation. The higher effectiveness of  $H^+$  in promoting the aggregation is reflected in the much less dense structure (DLCCA) that originated in the absence of  $Na^+$ . The observation of a more compact structure (RLA) in aggregates grown in the presence of  $Na^+$  can be suggestive either of its different ability with respect to the proton in screening the interaction potential between charged particles or of some specific interaction of this cation with the porphyrin.

**Acknowledgment.** We thank the CNR, MURST, Programmi di Ricerca Scientifica di Rilevante Interesse Nazionale, Cofinanziamento 1998-99 and INFN/PRA for financial support.

## References and Notes

- (1) *Structure and Dynamics of Strongly Interacting Colloids and Supramolecular Aggregates in Solution*; Chen, S. H.; Huang, J. S.; Tartaglia, P., Eds.; Luwer: Dordrecht, 1992.
- (2) *Scaling Concepts and Complex Fluids*, Mallamace, F., Ed.; Compositori: Bologna, 1995.
- (3) Lehn, J. M. *Supramolecular Chemistry*; VCH: Weinheim, 1995.
- (4) White, W. I. In *The Porphyrins*; Dolphin, D., Ed.; Academic: New York, 1978; Vol. 5, Chapter 7.
- (5) Hunter, C. A.; Sanders, M. K. *J. Am. Chem. Soc.* **1990**, *112*, 5525.
- (6) Kano, K.; Minamizono, H.; Kitae, T.; Negi, S. *J. Phys. Chem.* **1997**, *101*, 6118.
- (7) Deisenhofer, J.; Epp, O.; Miki, K.; Huber, R.; Michel, H. *J. Mol. Biol.* **1984**, *180*, 385.
- (8) Deisenhofer, J.; Epp, O.; Miki, K.; Huber, R.; Michel, H. *Nature*, **1985**, *318*, 618.
- (9) Katz, J. J.; Norris, J. R.; Shipman, L. L.; Thurnauer, M. C.; Wasielewski, M. R. *Annu. Rev. Biophys. Bioeng.* **1978**, *7*, 393.
- (10) Ravikanth, M.; Chandrashekar, T. K. *Struct. Bonding (Berlin)* **1995**, *82*, 105.
- (11) Kuhlbrandt, W. *Nature* **1995**, *374*, 497.
- (12) Schenning, A. P. H. J.; Benneker, F. B. G.; Geurts, H. P. M.; Liu, X. Y.; Nolte, R. J. M. *J. Am. Chem. Soc.* **1996**, *118*, 8549.
- (13) Hofkens, J.; Latterini, L.; Vanoppen, P.; Faes, H.; Jeuris, K.; Defeyter, S.; Kerimo, J.; Barbara, P. F.; Deschryver, F. C.; Rowan, A. E.; Nolte, R. J. M. *J. Phys. Chem. B* **1997**, *101*, 10588.
- (14) Gibbs, E. J.; Tinoco, I. Jr.; Maestre, M. F.; Ellinas, P. A.; Pasternack, R. F. *Biochem. Biophys. Res. Commun.* **1988**, *157*, 350.
- (15) Pasternack, R. F.; Bustamante, C.; Collings, P. J.; Giannetto, A.; Gibbs, E. J. *J. Am. Chem. Soc.* **1993**, *115*, 5393.
- (16) Mukundan, N. E.; Petho, G.; Dixon, D. W.; Kim, M. S.; Marzilli, L. G. *Inorg. Chem.* **1994**, *33*, 4676.
- (17) Pasternack, R. F.; Brigandi, R. A.; Abrams, M. J.; Williams, A. P.; Gibbs, E. J. *Inorg. Chem.* **1990**, *29*, 4483.
- (18) Pasternack, R. F.; Gurrieri, S.; Lauceri, R.; Purrello, R. *Inorg. Chim. Acta* **1996**, *246*, 7.
- (19) Pancoska, P.; Urbanova, M.; Bednarova, L.; Vacek, K.; Panschenko, V. Z.; Vasiliev, S.; Malon, P.; Kral, M. *Chem. Phys.* **1990**, *147*, 401.
- (20) Nezu, T.; Ebert, G. *Biopolymers* **1991**, *31*, 1257.
- (21) Gibbs, E. J.; Pasternack, R. F. *J. Inorg. Organomet. Polym.* **1993**, *3*, 77.
- (22) Purrello, R.; Monsù Scolaro, L.; Bellacchio, E.; Gurrieri, S.; Romeo, A. *Inorg. Chem.* **1998**, *37*, 3647.
- (23) Purrello, R.; Monsù Scolaro, L.; Lauceri, R.; Gurrieri, S.; Romeo, A. *J. Am. Chem. Soc.* **1998**, *120*, 12353.
- (24) Ohno, O.; Kaizu, Y.; Kobayashi, H. *J. Chem. Phys.* **1993**, *99*, 4128.
- (25) Ribò, J. M.; Crusats, J.; Farrera, J. A.; Valero M. L. *J. Chem. Soc., Chem. Commun.* **1994**, 681.
- (26) Pasternack, R. F.; Schaefer, K. F.; Hambright, P. *Inorg. Chem.* **1994**, *33*, 2062.
- (27) Akins, D. L.; Zhu, H.-R.; Guo, C. *J. Phys. Chem.* **1994**, *98*, 3612.
- (28) Maiti, N. C.; Ravikanth, M.; Mazumdar, S.; Periasamy, N. *J. Phys. Chem.* **1995**, *99*, 17192.
- (29) Akins, D. L.; Zhu, H.-R.; Guo, C. *J. Phys. Chem.* **1996**, *100*, 5420.
- (30) Barber, D. C.; Freitag-Beeston, R. A.; Whitten, D. G. *J. Phys. Chem.* **1991**, *95*, 4074.
- (31) Rubires, R.; Crusats, J.; El-Hachemi, Z.; Jaramillo, T.; Lopez, M.; Valls, E.; Farrera, J. A.; Ribò, J. M. *New J. Chem.* **1999**, 189.
- (32) Collings, P. J.; Gibbs, E. J.; Starr, T. E.; Vafek, O.; Yee, C.; Pomerance, L. A.; Pasternack, R. F. *J. Phys. Chem. B* **1999**, *103*, 8474.
- (33) Mobius, D. *Acc. Chem. Res.* **1981**, *14*, 63.
- (34) Nakahara, H.; Fukuda, K.; Mobius, D.; Kuhn, H. *J. Phys. Chem.* **1986**, *90*, 6144.
- (35) Valdes-Aguilera, O.; Neckers, D. C. *Acc. Chem. Res.* **1989**, *22*, 171.
- (36) Hessemann, J. *J. Am. Chem. Soc.* **1980**, *102*, 2176.
- (37) Fukuda, K.; Nakahara, H. *J. Colloid Interface Sci.* **1984**, *98*, 555.
- (38) McRae, E. G.; Kasha, M. In *Physical Processes in Radiation Biology*; Augenstein, L.; Mason, R.; Rosenberg, B., Eds.; Academic: New York, 1964; pp 23-42.
- (39) McRae, E. G.; Kasha, M. *J. Chem. Phys.* **1958**, *28*, 721.
- (40) Knapp, E. W. *Chem. Phys.* **1984**, *85*, 73.
- (41) Pasternack, R. F.; Collings, P. J. *Science* **1995**, *269*, 935.
- (42) Parkash, J.; Robblee, J. H.; Agnew, J.; Gibbs, E.; Collings, P.; Pasternack, R. F.; de Paula, J. C. *Biophys. J.* **1998**, *74*, 2089.
- (43) Mallamace, F.; Micali, N.; Trusso, S.; Monsù Scolaro, L.; Romeo, A.; Terracina, A.; Pasternack, R. F. *Phys. Rev. Lett.* **1996**, *76*, 4741.
- (44) Monsù Scolaro, L.; Romeo, A.; Mallamace, F.; Micali, N.; Purrello, R. *Il Nuovo Cimento* **1998**, *20D*, 2207.
- (45) Micali, N.; Monsù Scolaro, L.; Romeo, A.; Mallamace, F. *Phys. Rev. E* **1998**, *57*, 5766.
- (46) Mallamace, F.; Monsù Scolaro, L.; Romeo, A.; Micali, N. *Phys. Rev. Lett.* **1999**, *59*, 3480.
- (47) *On Growth and Form*, Stanley, H. E.; Ostrowsky, N. Eds.; NATO ASI Series, Martinus Nijhoff Publishers: Dordrecht, 1986.
- (48) Mandlbrot, B. *Fractals, Form and Dimensions*, Freeman: San Francisco, 1977.
- (49) Vicsek, T. *Fractal Growth Phenomena*, World Scientific: London, 1992.
- (50) Berne, B. J.; Pecora, R. *Dynamic Light Scattering*; Wiley: New York, 1976.
- (51) Martin, J. E.; Akerson, B. J. *Phys. Rev. A* **1985**, *31*, 1180.
- (52) Mallamace, F.; Micali, N. *Rivista del Nuovo Cimento* **1992**, *15*, 1.
- (53) Lawson, C. L.; Hanson, R. J. *Solving Least Squares Problems*; Prentice Hall: Englewood Cliffs, NJ, 1974.
- (54) Grabowski, E. F.; Morrison, I. D. In *Measurements of Suspended Particles by Quasi-Elastic Light Scattering*; Dahneke, B. E., Ed.; Wiley-Interscience: New York, 1986; p 199.
- (55) Chandrashekar, T. K.; van Willigen, H.; Ebersole, M. H. *J. Phys. Chem.* **1984**, *88*, 4326.
- (56) Kalyanasundaram, K. In *Photochemistry of Polypyridine and Porphyrin Complexes*; Academic: London, 1992; p 428.
- (57) Chen, S. H.; Teixeira, J. *Phys. Rev. Lett.* **1986**, *57*, 2583.
- (58) To rule out the possibility that the faster contribution could be ascribed to experimental artifact, we performed DLS experiments on aggregated samples filtered through 0.2- $\mu$ m Millipore filters. The correlograms still evidence the presence of small objects with hydrodynamic radii of  $\sim 5$  nm.
- (59) Edward, J. T. *J. Chem. Edu.* **1970**, *47*, 261.
- (60) Verwey, E. J.; Overbeek, J. Th. G. *Theory of the Stability of Lyophobic Colloids*; Elsevier: Amsterdam, 1948.
- (61) Derjaguin, B. V.; Landau, L. *Acta Phys. Chim. Debricina* **1941**, *14*, 633.
- (62) Hamaker, H. C. *Physica* **1937**, *4*, 1058.
- (63) Ottewill, R. H. *Sp. Rep. Chem. Soc. Colloid Sci.* **1973**, *1*, 175.
- (64) Chandrasekhar, S. *Rev. Mod. Phys.* **1943**, *15*, 1.
- (65) Kolb, M.; Jullien, R. *J. Phys. Lett.* **1984**, *46*, L977.
- (66) Jullien, R.; Kolb, M. *J. Phys. A* **1984**, *17*, L369.
- (67) Weitz, D. A.; Huang, J. S.; Lin, M. Y.; Sung, J. *Phys. Rev. Lett.* **1984**, *53*, 1657.
- (68) Weitz, D. A.; Huang, J. S.; Lin, M. Y.; Sung, J. *Phys. Rev. Lett.* **1985**, *54*, 141.